Available online at www.sciencedirect.com
SCIENCE DIRECT®
Icarus 169 (2004) 492–498
ICARUS
www.elsevier.com/locate/icarus

Zonal jets in rotating convection with mixed mechanical boundary conditions

Jonathan M. Aurnou [a,*] and Moritz H. Heimpel [b]

[a] *Department of Terrestrial Magnetism, Carnegie Institution of Washington, Washington, DC 20015-1305, USA*
[b] *Department of Physics, University of Alberta, Edmonton AB, T6G 2J1, Canada*

Received 22 August 2003; revised 15 January 2004

Available online 9 April 2004

Abstract

Large-scale zonal flows, as observed on the giant planets, can be driven by thermal convection in a rapidly rotating spherical shell. Most previous models of convectively-driven zonal flow generation have utilized stress-free mechanical boundary conditions (*FBC*) for both the inner and the outer surfaces of the convecting layer. Here, using 3D numerical models, we compare the *FBC* case to the case with a stress free outer boundary and a non-slip inner boundary, which we call the mixed case (*MBC*). We find significant differences in surface zonal flow profiles produced by the two cases. In low to moderate Rayleigh number *FBC* cases, the main equatorial jet is flanked by a strong, high-latitude retrograde jets in the northern and southern hemispheres. For the highest Rayleigh number *FBC* case, the equatorial jet is flanked by strong reversed jets as well as two additional large-scale alternating jets at higher latitudes. The *MBC* cases feature stronger equatorial jets but, much weaker, small-scale alternating zonal flows are found at higher latitudes. Our high Rayleigh number *FBC* results best compare with the zonal flow pattern observed on Jupiter, where the equatorial jet is flanked by strong retrograde jets as well as small-scale alternating jets at high latitude. In contrast, the *MBC* results compare better with the observed flow pattern on Saturn, which is characterized by a dominant prograde equatorial jet and a lack of strong high latitude retrograde flow. This may suggest that the mechanical coupling at the base of the jovian convection zone differs from that on Saturn.

Keywords: Jupiter; Saturn; Atmospheres; Convection

1. Introduction

Understanding how large-scale zonal winds are generated on the giant planets is a longstanding problem in planetary and geophysical fluid dynamics (Busse, 1976; Cho and Polvani, 1996a). As shown in Fig. 1, strong eastward jets dominate the equatorial regions of both Jupiter and Saturn. At higher latitudes, much weaker eastward- and westward-directed flows are found on Jupiter. On Saturn, the high latitude flow consists of a smaller number of almost purely eastward-directed zonal jets. Galileo probe measurements made to a depth of 125 km below the cloud deck showed that the jovian winds extend into the planets interior, well below the shallow layer heated by solar insolation (Atkinson et al., 1998). These observations suggest that the large-scale zonal winds on the giant planets may be generated by deep convection. In addition to the observable near-surface winds on the giant planets, studies of planetary core dynamics has shown that the existence of large-scale zonal flows may also be necessary to maintain dynamo action (Gubbins and Roberts, 1987).

The deep atmospheric convection zones of the giant planets are believed to extend down to the depth of metalization of the hydrogen-rich fluid. Estimates of the metallic hydrogen transition depths are at roughly 0.7–0.9 of Jupiter's radius and 0.4–0.6 of Saturn's radius (Guillot, 1999). It has been proposed that the metallic transition acts as a vertical barrier across which convection cannot occur due to the increase in fluid density that accompanies the change in phase (Stevenson and Salpeter, 1977). Convection also occurs below the transition, driving the planetary dynamos in these metalized regions. Any zonal flows will be strongly retarded by the action of Lorentz forces in the vicinity of the metal-

* Corresponding author. Present address: Department of Earth and Space Sciences, 5690 Geology Bldg., UCLA, Los Angeles, CA 90095-1567, USA.
E-mail address: aurnou@ucla.edu (J.M. Aurnou).

0019-1035/$ – see front matter
doi:10.1016/j.icarus.2004.01.013

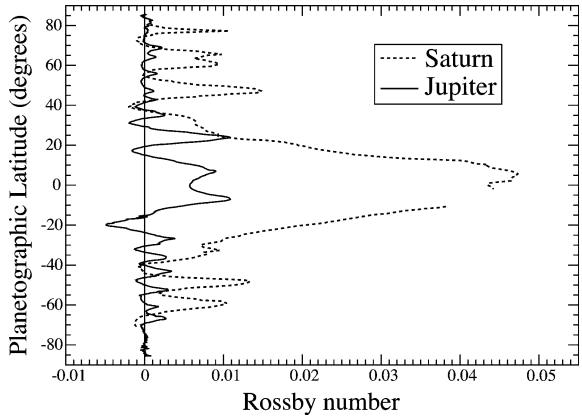

Fig. 1. Surface zonal flow observations of Jupiter (solid line) and Saturn (dashed line) plotted as a function of planetographic latitude. Non-dimensional velocities are given in Rossby number units, $Ro = u/\Omega r_o$. Here we use the equatorial planetary radii for r_o. Adapted from Porco et al. (2003) and Sanchez-Lavega et al. (2000).

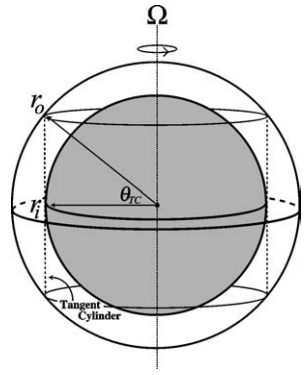

Fig. 2. Schematic showing a spherical shell with a radius ratio $\chi = r_i/r_o = 0.75$. The tangent cylinder intersects the outer surface, r_o, at $\theta_{\rm TC} = \pm\cos^{-1}\chi = \pm 41^\circ$ latitude.

ization transition (Kirk and Stevenson, 1987). In addition, the convection zones of the giant planets are many density scale heights deep. Zhang and Schubert (2000) have shown that moderate compressibility effects need not destroy the geostrophy of rotating convective flows. However, conservation of momentum will tend to cause the amplitude of zonal winds to decrease as the fluid density increases with depth in the convection zone. Therefore, zonal flows at the base of the deep convection zone are likely to be sluggish relative to the rapid winds measured at the surface, so that the bottom of the deep convection zone may be approximated as a stationary boundary in the rotating reference frame defined by the planetary magnetic field. The lack of strong, measurable secular variation of the jovian magnetic field supports this approximation (Russell et al., 2001).

Studies of rapidly-rotating convection have found that convection tends to occur dominantly in the form of quasi-geostrophic columns aligned in the direction of the rotation axis (Roberts, 1968; Busse, 1970; Jones et al., 2000). The convection columns first form outside the imaginary, right cylinder, referred to as the tangent cylinder, that circumscribes the equator of the inner spherical boundary of the fluid volume (see Fig. 2). Near the onset of convection, the geostrophic "cartridge belt" convective planform generates net Reynolds stresses (Busse, 1976; Zhang, 1992; Cardin and Olson, 1994). These stresses transfer net positive angular momentum outward and negative angular momentum inward. Because the flow is geostrophic, the Reynolds stresses drive zonal flows that do not vary strongly in the axial direction.

It is known that rigid inner and outer boundaries inhibit the production of zonal flows, whereas strong zonal flows develop for stress-free inner and outer boundaries (Aurnou and Olson, 2001). Studies of freely-evolving shallow layer or two-dimensional turbulence on a spherical shell have been used to simulate flows in the Earth's oceans, atmosphere, and on the giant planet cloud decks (Cho and Polvani, 1996a, 1996b; Rhines, 1975; Yoden and Yamada, 1993). A shallow layer parameter study applied to Jupiter (Cho and Polvani, 1996b) reproduced several generic features of the giant planets, including multiple alternating jets, vortices, and a strong equatorial flow; although the equatorial flow was retrograde, opposite in direction to the observed prograde equatorial flows on Jupiter and Saturn. Experimental studies of rotating convection at high Rayleigh number and low Ekman number found that zonal flows can develop with two rigid boundaries (Manneville and Olson, 1996; Aubert et al., 2001). However, in these studies, strong prograde equatorial jets were not observed. Most of the recent studies relevant to zonal flow generation on the giant planets have focused on deep convection in a rapidly rotating spherical shell bounded by stress-free boundaries (Zhang, 1992; Sun et al., 1993; Ardes et al., 1997; Tilgner and Busse, 1997; Christensen, 2001, 2002; Wicht et al., 2002; Yano et al., 2003). In these studies, Reynolds stresses, which are balanced only by weak viscous forces, drive strong prograde jets at low, equatorial latitudes and retrograde jets at higher latitudes. In strongly supercritical rotating convection with stress-free boundaries, Christensen (2001) has shown that alternating, large-scale, east–west zonal jets can be generated at high latitudes when convection becomes vigorous within the tangent cylinder. In truncated models of high latitude convection, Jones et al. (2003) found that the formation of multiple, small-scale alternating jets was facilitated in cases in which they assume strong magnetic fields produce a rigid lower mechanical boundary condition while leaving the outer boundary mechanically stress-free.

Here we carry out a study of deep layer rotating spherical shell convection, similar to the low resolution work of Gilman (1978), in which we compare cases with stress-free boundary conditions against "mixed" cases where the outer boundary is stress-free and the inner boundary is rigid. In the following section we will outline the numerical methods used in this study. In Section 3 we present the results from the simulations. Lastly, in Section 4, we discuss our results and compare them to the gross features of the observed zonal flows on the giant planets.

2. Numerical methods and models

We study the convective response of a layer of Boussinesq fluid in a rapidly rotating, three-dimensional spherical shell geometry subject to isothermal temperature boundary conditions. Gravity varies linearly with radius, with value g_o on the outer boundary at r_o. The simulations have been carried out in a spherical shell of fluid such that the inner/outer radius ratio $\chi = r_i/r_o = 0.75$, where r_i is the inner boundary radius (see Fig. 2). This radius ratio is geometrically similar to estimates for the deep atmosphere of Jupiter (Guillot, 1999). We do not simulate the convection in the outermost atmosphere affected by solar insolation or in the fluid interior to r_i, which represents the metallic transition depth.

We numerically integrate the Navier–Stokes equation and the heat equation

$$E\left(\frac{\partial \mathbf{u}}{\partial t} + \mathbf{u}\cdot\nabla\mathbf{u} - \nabla^2\mathbf{u}\right) + 2\hat{z}\times\mathbf{u} = -\nabla p + \left(\frac{RaE}{Pr}\right)\frac{\mathbf{r}T}{r_o}, \quad (1)$$

$$\frac{\partial T}{\partial t} + \mathbf{u}\cdot\nabla T = \left(\frac{1}{Pr}\right)\nabla^2 T, \quad (2)$$

subject to the continuity condition

$$\nabla\cdot\mathbf{u} = 0, \quad (3)$$

where $\mathbf{u}$ is the velocity vector, p is the pressure, and T is the temperature. Equations (1)–(3) have been non-dimensionalized using the temperature difference ΔT across the shell thickness $D = r_o - r_i = r_o(1-\chi)$ which is used as the length scale, D^2/ν for time-scale, where ν is the kinematic viscosity, ν/D for the velocity-scale, and $\rho\Omega\nu$ for the pressure-scale, where ρ is the fluid density, and Ω is the angular rotation rate. This scaling produces the following non-dimensional control parameters:

$$E = \frac{\nu}{\Omega D^2}; \qquad Pr = \frac{\nu}{\kappa}; \qquad Ra = \frac{\alpha g_o \Delta T D^3}{\nu\kappa}, \quad (4)$$

where α is the thermal expansivity and κ is the thermal diffusivity.

The Ekman number, E, is defined in Eq. (4) as the ratio of viscous to Coriolis forces and is fixed at a value of 3×10^{-4} in the majority of the calculations presented here. The Prandtl number, Pr, which is a physical property of the fluid, is maintained at unity in our calculations. The Rayleigh number represents the strength of buoyancy forces in the fluid. Convection occurs only for Rayleigh numbers greater than the critical Rayleigh number, Ra_C. As Ra is increased above Ra_C, convection becomes increasingly vigorous. For both sets of boundary conditions, *FBC* and *MBC*, $Ra_C \simeq 10^5$ at $E = 3\times10^{-4}$ and $Pr = 1$. In this study we will focus on the two cases $Ra = 10Ra_C$ and $Ra = 30Ra_C$. Following the work of Aubert et al. (2001) and Christensen (2002), we will also present some of our results in terms of the modified Rayleigh number $Ra^* = RaE^2/Pr = \alpha g_o \Delta T/\Omega^2 D$, for which Christensen (2002) has derived asymptotic scaling laws for rotating convection in a $\chi = 0.35$ spherical shell geometry subject to stress-free boundary conditions. Christensen (2002) arrives at this modified Rayleigh number by using $1/\Omega$ as the characteristic timescale in non-dimensionalizing the equations of motion. The advantage of this scaling is that Ra^* does not depend on any microscopic transport properties of the fluid that appear not to control the convection in the asymptotic low E, high Ra regime (Aubert et al., 2001). Although our parameter values are many orders of magnitude from estimates for the giant planets, the asymptotic laws of Christensen (2002) suggest that our simulations may not be very far from the asymptotic regime. Thus, we will later compare our results against observations of the planets, while still keeping in mind that Christensen's (2002) scaling laws may or may not hold at far more extreme planetary parameter values.

A critical output parameter from the calculations is the Rossby number

$$Ro = ReE(1-\chi) = \frac{u}{\Omega r_o}, \quad (5)$$

which is the fluid velocity non-dimensionalized by the equatorial rotation rate of the outer boundary. Here the Reynolds number $Re = uD/\nu$ is the non-dimensional flow velocity output from our calculations. Peak Rossby number values for our calculations reach ~ 0.12, which is far larger than the observed peak values of ~ 0.01 and 0.05 for Jupiter and Saturn, respectively.

Equations (1)–(3) are solved using the pseudo-spectral technique of Glatzmaier (1984). Chebyshev polynomials are used in the radial direction on 81 radial levels. Spherical harmonics are used on spherical surfaces with 576 nodes in longitude and 288 nodes in latitude. The spherical harmonic expansion is truncated at degree and order of 192. We initialize all our calculations by randomly perturbing the temperature field. Solutions are integrated until they reach a statistically-steady-state, typically after 5–10 viscous diffusion timescales. To lessen the total computational expense, we have imposed 4-fold longitudinal symmetry on our solutions. Calculations of Ra_C in spherical shells have shown that 4-fold symmetry does not strongly affect the high wavenumber convection that develops in spherical shells with $\chi > 0.4$ (Al-Shamali et al., 2004). More detailed descriptions of the numerical technique can be found in Christensen et al. (1999). Hyperdiffusivities are not employed in these calculations. In the *FBC* cases, in which both the inner and outer mechanical boundary conditions are stress-free, angular momentum is conserved in the fluid layer to within $\sim 1\%$. In *MBC* cases, where the inner boundary is rigid and the outer boundary is stress-free, angular momentum is not conserved because the rigid inner boundary can apply viscous torques to the fluid and Ω is held fixed.

3. Results

Figure 3 shows plots of the azimuthally-averaged surface zonal flows (a, c) and the azimuthally-averaged zonal

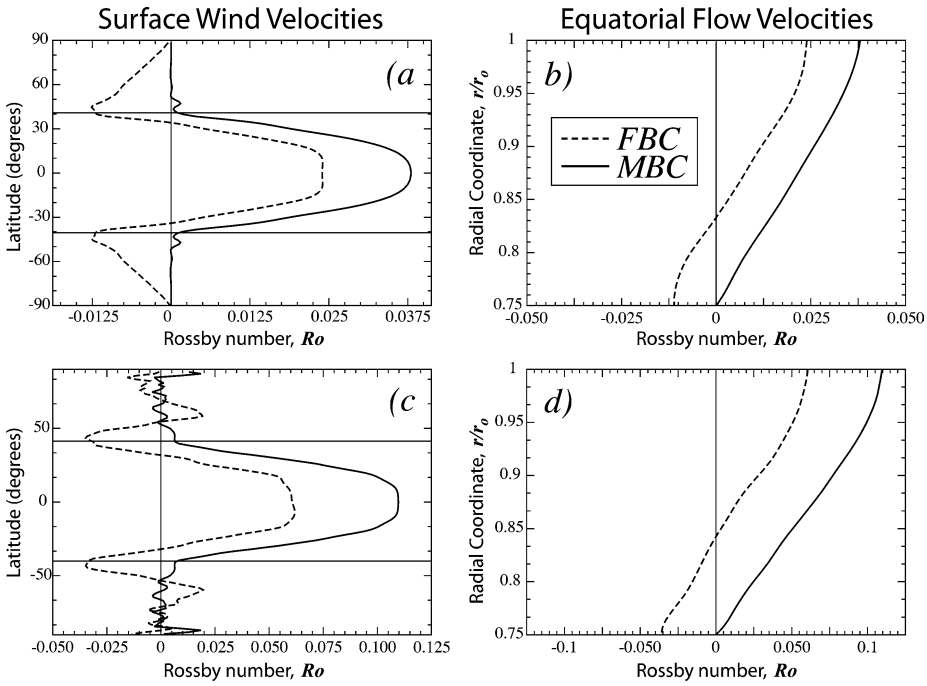

Fig. 3. Plots of zonally-averaged azimuthal velocity. Left column (a), (c): surface winds versus latitude; right column (b), (d): equatorial plane velocities plotted versus radius. Top row (a), (b): $10Ra_C$; bottom row (c), (d): $30Ra_C$. Solid lines: *MBC* results (rigid inner boundary, stress-free outer boundary); dashed lines: *FBC* results (stress-free boundaries). All velocities are given in *Ro* units. Thin horizontal lines in *a* and *c* denote the tangent cylinder latitude, $\pm\theta_{\rm TC}$.

velocities in the equatorial plane (b, d). Dashed lines correspond to *FBC* cases. Solid lines correspond to *MBC* cases. Figure 3a shows the surface azimuthal zonal wind profiles generated in cases with $Ra = 10^6 \simeq 10Ra_C$. In the *FBC* case, a large prograde equatorial jet is formed with a peak $Ro = 0.024$. Flanking this prograde jet are two large retrograde jets that form near the tangent cylinder latitude of $\theta_{\rm TC} = \pm\cos^{-1}(\chi) = \pm 41°$. In marked contrast, the *MBC* case features a stronger equatorial jet with peak $Ro = 0.038$ and no flanking retrograde jets at high latitudes. Instead of retrograde jets, mixed boundary conditions produce weak, small-scale, high latitude zonal flows that are similar to the high latitude results from calculations with two rigid boundaries (Aurnou and Olson, 2001). In the *FBC* case, 90% of the kinetic energy is located in the zonal flow field. The zonal flow contains 95% of the total kinetic energy in the *MBC* case. Similar calculations with rigid outer boundaries typically contain less than 10% of the kinetic energy in their zonal flow fields.

The equatorial azimuthal zonal flow profiles for the $Ra \simeq 10Ra_C$ cases are plotted in Fig. 3b. The *FBC* and *MBC* profiles are similar in shape, but in the *MBC* case the zonal flow is zero at the inner boundary whereas the *FBC* case features a retrograde flow at r_i. This similarity of the equatorial profiles demonstrates that the structure of convection outside the tangent cylinder is remains largely unaffected by the choice of inner mechanical boundary condition.

Figure 3c shows the surface azimuthal zonal wind profiles in cases with $Ra = 3 \times 10^6 \simeq 30Ra_C$. Additional images of the azimuthal velocity field on r_o are shown in Figs. 4a, 4b. In case *FBC*, the prograde equatorial jet has a peak $Ro = 0.06$. In addition, strong convection within the tangent cylinder now drives a set of alternating jets at high latitude, very similar to the pattern found by Christensen (2001). Here the *MBC* case features an equatorial jet with peak $Ro = 0.11$ and numerous small-scale jets at high latitudes, in basic agreement with the high latitude *MBC*-like models of Jones et al. (2003) as well as with shallow layer models such as those of Rhines (1975), Williams (1978), and Yoden and Yamada (1993). Similar small-scale, high-latitude jet structures are found in $Ra = 3 \times 10^6$ calculations made with two rigid boundaries. The zonal kinetic energy fractions are 94 and 89% for the *MBC* and *FBC* cases, respectively.

The results in Fig. 3d are similar to those in panel (b). The *MBC* profile can be reproduced by shifting the *FBC* profile forward such that no retrograde zonal motion occurs at r_i.

Figure 5 shows the results from *MBC* calculations at $E = 10^{-4}$ and $Ra = 10^7$. An equatorial jet forms with a peak $Ro = 0.068$, while convection in the tangent cylinder interior drives small-scale, high-latitude alternating flows. Downwelling flows at the poles drive the polar vortex structures there. In this lower Ekman number case, the modified Rayleigh number takes on the value of $Ra^* = 0.10$. This value is very close to the case with $E = 3 \times 10^{-4}$ and $Ra = 10^6$, where $Ra^* = 0.09$. We find similar results in these two *MBC* cases. In both, a prograde equatorial jet develops with very weak alternating flows at high latitudes because convection is not yet vigorous in the tangent cylinder interior. The peak equatorial jet Rossby number is ~ 0.07 for

the $E = 10^{-4}$ case and ~ 0.04 for the $E = 3 \times 10^{-4}$ case, in good agreement with Christensen (2002). These results show that at lower Ekman number and comparable convective vigor, a stronger equatorial jet develops, accompanied by finer-scale high-latitude zonal flow structures.

4. Discussion

Large-scale equatorial jets form for both the mixed boundaries case and the free boundaries case. However, at high latitudes these two cases markedly differ: strong retrograde jets develop in the *FBC* cases in order to conserve angular momentum in the fluid layer, whereas in the *MBC* case viscous torques at the non-slip inner boundary act on the adjacent fluid to spin it up to the imposed rotation rate Ω. In the $Ra \leqslant 10Ra_C$ cases with two rigid boundary conditions studied by Aurnou and Olson (2001), weak convection within the tangent cylinder generates small-scale alternating zonal flows such that all the high latitude fluid remains close to the rotation rate Ω. Here, the $Ra \leqslant 10Ra_C$ *MBC* case produces a flow pattern that resembles the superposition of the *FBC* velocity (or Rossby number) profile at low latitudes with the high latitude velocity profile of rigid boundary calculations (which are not presented in this paper). This implies that the fluid convection outside the tangent cylinder is strongly affected by the outer boundary condition, which is stress-free for the *MBC* case, whereas inside the tangent cylinder the convection pattern is more strongly controlled by the rigid inner boundary.

The *MBC* cases feature peak prograde *Ro* and zonal kinetic energy percentages that are higher than respective *FBC* cases. These differences occur because the non-slip inner boundary in the *MBC* cases acts to torque forward the entire equatorial jet structure until the viscous stresses are zero at r_i. However, the peak-to-trough differences in zonal equatorial velocity are identical for the *MBC* and *FBC* cases for $Ra \leqslant 10Ra_C$. For $10Ra_C < Ra \leqslant 30Ra_C$, the peak-to-trough velocity difference for the *MBC* case monotonically increases over the *FBC* case by up to 10%. This difference is caused by the different flows that develop within the tangent cylinder depending on the mechanical boundary conditions.

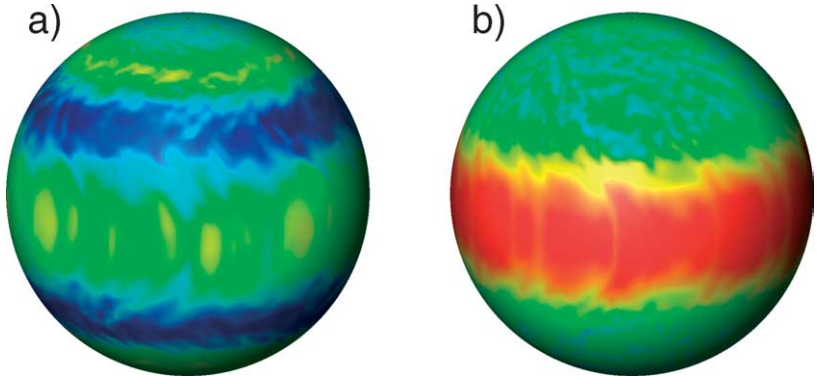

Fig. 4. Azimuthal velocity on the outer boundary, r_o, for $E = 3 \times 10^{-4}$ and $Ra = 3 \times 10^6 \simeq 30Ra_C$. (a) *FBC*; (b) *MBC*. Red represents prograde flow (eastward flow; positive *Ro*); blue represents retrograde flow (westward flow; negative *Ro*). The same color scale is used in (a) and (b).

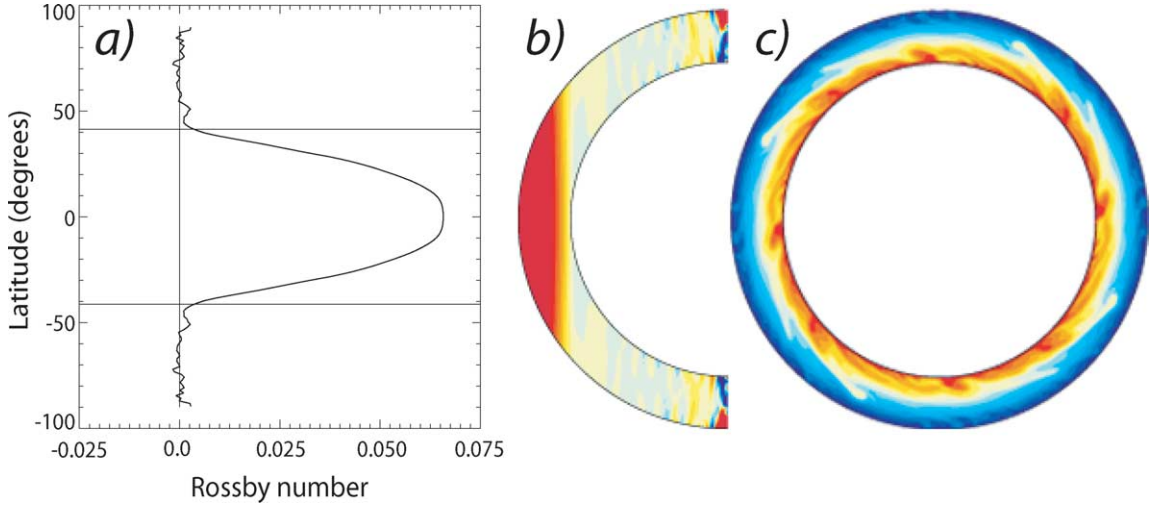

Fig. 5. Plots of (a) zonally-averaged azimuthal surface velocity versus latitude, (b) meridional slice of zonally-averaged angular velocity, and (c) equatorial temperature contours viewed from the northern pole for the *MBC* case with $E = 10^{-4}$ and $Ra = 10^7$.

We note that the total angular momentum is greater in the *MBC* cases than in the *FBC* cases because we hold the rotation rate of the bottom boundary fixed in all of the calculations. If we held the total angular momentum fixed, instead of the value of Ω, we would expect to find smaller differences in peak *Ro* and zonal energy percentage between *MBC* and *FBC* cases. However, the choice of mechanical boundary conditions does result in fundamental differences in the zonal flow pattern relative to the rotating reference frame. It is these fundamental differences in the flow pattern that are most relevant for comparisons with the planetary observations.

4.1. Comparison to observed flows on the giant planets

The equatorial jets that form for the *MBC* and *FBC* cases may be crudely compared to the broadest-scale structure of the low latitude flows on both Jupiter and Saturn. Our simulations capture none of the shallow vortex structures, the dips in the equatorial jet cores or the precise jet amplitudes or widths. In addition, the asymmetry in the jovian profile, due to the Great Red Spot, increases the difficulty in comparing the profiles from our simulations with the equatorial region of Jupiter. It is nonetheless clear that the overall jovian flow structure within $\pm 20^\circ$ latitude is that of a large-scale prograde jet with a peak $Ro \sim 0.05$, which agrees with our results at low latitudes (i.e., outside the tangent cylinder). Surrounding the jovian equatorial jet are narrow but relatively strong retrograde jets. At higher latitudes on Jupiter, small-scale alternating, zonal flows are observed, which are slightly skewed in the prograde direction. On Saturn the equatorial jet is surrounded in each hemisphere by two or three large-scale, dominantly prograde, high latitude jets.

The results of our simulations suggest that the equatorial jets may demarcate the region exterior to the tangent cylinder. Using the data shown in Fig. 1, we approximate the latitudinal extent of Jupiter's equatorial jet to be $\pm 20^\circ$ and Saturn's equatorial jet to be $\pm 40^\circ$. These provide estimates of the convection zone radius ratio, via the relation $\chi = \cos\theta_{\mathrm{TC}}$, of ~ 0.9 and ~ 0.75 for Jupiter and Saturn, respectively. These dynamically-based results are in basic agreement with range of estimates for the base of the jovian convection zone but are significantly higher than current estimates for Saturn (Guillot, 1999), suggesting that the effective base of the zonal flow generation region on Saturn may be strongly effected by magnetic fields or compressibility effects. Clearly, simulations over a range of χ should be carried out to determine which spherical shell geometries best fit the equatorial jet observations.

The *FBC* results at $10Ra_C$ do not compare well with the observed high latitude surface flows on either Jupiter or Saturn, both of which lack the large-scale retrograde flow that dominates the high latitude regions in this case (see Fig. 3a).

The $30Ra_C$ *FBC* results compare better with the zonal flow profile for Jupiter. The equatorial jet and the relatively narrow, flanking retrograde jets that form along the tangent cylinder are similar to the jovian profile for latitudes below $\pm 30^\circ$ latitude. The pair of large-scale, alternating jets that form in the tangent cylinder interior in this case have larger spatial length scales than the flows in the jovian high latitude observations. This difference in length scale may be expected for the low *Ra* and high *E* used in our calculations relative to their far more extreme planetary values. Additionally, we find that the *MBC* results are comparable to the most recent polar observations of Jupiter made by the Cassini probe, which show fine-scale, alternating jets at very high latitude (Porco et al., 2003).

The *MBC* calculations, which feature a large-scale prograde jet at low latitudes with little retrograde flow at high latitudes, compare better with the zonal flows observed on Saturn. Alternating large-scale jets form in the $Ra = 3 \times 10^6$ *FBC* case that are similar in relative length scale and magnitude (but not direction) to the prograde high latitude jets observed on Saturn. Although our *MBC* calculations are unable to produce strongly prograde, large-scale, high latitude jets, as are observed on Saturn, further studies made at higher *Ra* and lower *E* may generate such flow patterns. We see some tendency for high latitude jets to form as *E* is scaled down by comparing Figs. 3a and 5a. Those figures represent two cases that have a similar modified Rayleigh number value ($Ra^* \simeq 0.10$). Note that in Fig. 3a there is very little motion within the tangent cylinder, whereas in Fig. 5 small-scale zonal flows exist. In contrast, the *MBC* case shown in Fig. 3c has $Ra^* = 0.27$ and the high-latitude jets are far stronger and larger in scale. Taken together our results indicate that, at lower *E* and comparable Ra^*, more realistic high latitude flows may be generated. At more extreme parameter values similar jets may become excited in the *MBC* cases, but, analogous to our present results, the effects of the rigid inner boundary may cause these flows to be strongly skewed in the prograde direction.

The *MBC* calculations, which lack strong retrograde flows at high latitude, are similar, at first order, to the zonal flow features on Saturn at both low and high latitude. However, quantitatively, the equatorial jet is too strong and the high latitude jets are too weak relative to the equatorial flows. The $30Ra_C$ *FBC* case compares well with the low-latitude jovian equatorial jet and its flanking, mid-latitude retrograde jets. This suggests that the effective mechanical coupling at the base of the convection zone may be weaker on Jupiter, and better approximated by a stress-free boundary condition, than on Saturn, where a rigid inner boundary condition may better apply. Clearly, both *MBC* and *FBC* cases deserve further study in order to understand how zonal flows can develop from deep convection on the giant planets.

Acknowledgments

Financial support for J.A. has been provided under NASA grants NAG5-4077 and NAG5-10165. Partial financial support for M.H. has been provided by the Natural Sciences

and Engineering Research Council (NSERC) of Canada. We thank Chris Jones and an anonymous referee for insightful reviews.

References

Al-Shamali, F.M., Heimpel, M.H., Aurnou, J.M., 2004. Varying shell geometry in rotating spherical shell convection. Geophys. Astrophys. Fluid Dynam. In press.

Ardes, M., Busse, F.H., Wicht, J., 1997. Thermal convection in rotating spherical shells. Phys. Earth Planet. In. 99, 55–67.

Atkinson, D.H., Pollack, J.B., Seiff, A., 1998. The Galileo Probe Doppler Wind Experiment: measurement of the deep zonal winds on Jupiter. J. Geophys. Res. 103, 22911–22928.

Aubert, J., Brito, D., Nataf, H.C., Cardin, P., Masson, J.P., 2001. A systematic experimental study of spherical shell convection in water and liquid gallium. Phys. Earth Planet. In. 128, 51–74.

Aurnou, J.M., Olson, P.L., 2001. Strong zonal winds from thermal convection in a rotating spherical shell. Geophys. Res. Lett. 28, 2557–2559.

Busse, F.H., 1970. Thermal instabilities in rapidly rotating systems. J. Fluid Mech. 44, 441–460.

Busse, F.H., 1976. A simple model of convection in the jovian atmosphere. Icarus 20, 255–260.

Cardin, P., Olson, P., 1994. Chaotic thermal convection in a rapidly rotating spherical shell: consequences for flow in the outer core. Phys. Earth Planet. In. 82, 235–259.

Cho, J.Y.-K., Polvani, L.M., 1996a. The morphogenesis of bands and zonal winds in the atmospheres on the giant outer planets. Science 273, 335–337.

Cho, J.Y.-K., Polvani, L.M., 1996b. The emergence of jets and vortices in freely evolving, shallow-water turbulence on a sphere. Phys. Fluids 8, 1531–1552.

Christensen, U.R., 2001. Zonal flow driven by deep convection on the major planets. Geophys. Res. Lett. 28, 2553–2556.

Christensen, U.R., 2002. Zonal flow driven by strongly supercritical convection in rotating spherical shells. J. Fluid Mech. 470, 115–133.

Christensen, U.R., Olson, P.L., Glatzmaier, G.A., 1999. Numerical modeling of the geodynamo: a systematic parameter study. Geophys. J. Int. 138, 393–409.

Gilman, P.A., 1978. Nonlinear dynamics of Boussinesq convection in a deep rotating spherical shell. III. Effects of velocity boundary conditions. Geophys. Astrophys. Fluid Dynam. 11, 181–203.

Glatzmaier, G.A., 1984. Numerical simulation of stellar convection dynamos. I. The model and method. J. Comput. Phys. 55, 461–484.

Gubbins, D., Roberts, P.H., 1987. Magnetohydrodynamics of the Earth's core. In: Jacobs, J.A. (Ed.), Geomagnetism, vol. 2. Academic Press, London.

Guillot, T., 1999. Interiors of giant planets inside and outside the Solar System. Science 286, 72–77.

Jones, C.A., Soward, A.M., Mussa, A.I., 2000. The onset of thermal convection in a rapidly rotating sphere. J. Fluid Mech. 405, 157–169.

Jones, C.A., Rotvig, J., Abdulrahman, A., 2003. Multiple jets and zonal flow on Jupiter. Geophys. Res. Lett. 30, 1731–1734.

Kirk, R.L., Stevenson, D.J., 1987. Hydromagnetic constraints on deep zonal flow in the giant planets. Astrophys. J. 316, 836–846.

Manneville, J.B., Olson, P., 1996. Banded convection in rotating fluid spheres and the circulation of the jovian atmosphere. Icarus 122, 242–250.

Porco, C.C., 23 colleagues, 2003. Cassini imaging of Jupiter's atmosphere, satellites and rings. Science 299, 1541–1547.

Rhines, P.B., 1975. Waves and turbulence on the beta-plane. J. Fluid Mech. 69, 417–441.

Roberts, P.H., 1968. On the thermal instability of a rotating-fluid sphere containing heat sources. Philos. Trans. R. Soc. London Ser. A 263, 93–117.

Russell, C.T., Yu, Z.J., Khurana, K.K., Kivelson, M.G., 2001. Magnetic field changes in the inner magnetosphere of Jupiter. Adv. Space Res. 28, 897–902.

Sanchez-Lavega, A., Rojas, J.F., Sada, P.V., 2000. Saturn's zonal winds at cloud level. Icarus 147, 405–420.

Stevenson, D.J., Salpeter, E.E., 1977. The phase diagram and transport properties for hydrogen–helium fluid planets. Astrophys. J. Suppl. 35, 221–237.

Sun, Z.P., Schubert, G., Glatzmaier, G.A., 1993. Banded surface flow maintained by convection in a model of the rapidly rotating giant planets. Science 260, 661–664.

Tilgner, A., Busse, F.H., 1997. Finite amplitude convection in rotating spherical fluid shells. J. Fluid Mech. 332, 359–376.

Wicht, J., Jones, C.A., Zhang, K., 2002. Instability of zonal flows in rotating shells: an application to Jupiter. Icarus 155, 425–435.

Williams, G.P., 1978. Planetary circulations. 1. Barotropic representation of jovian and terrestrial turbulence. J. Atmos. Sci. 35, 1399–1425.

Yano, J.I., Talagrand, O., Drossart, P., 2003. Origins of atmospheric zonal winds. Nature 421, 36.

Yoden, S., Yamada, M., 1993. A numerical experiment on two-dimensional decaying turbulence on a rotating sphere. J. Atmos. Sci. 50, 631–643.

Zhang, K., 1992. Spiraling columnar convection in rapidly rotating spherical shells. J. Fluid Mech. 236, 535–556.

Zhang, K., Schubert, G., 2000. Teleconvection: remotely driven thermally convection in rotating stratified spherical layers. Science 290, 1944–1947.